Environ. Sci. Technol. **2009,** *43,* 8184–8190

Secondary Organic Aerosol Formation by Self-Reactions of Methylglyoxal and Glyoxal in Evaporating Droplets

DAVID O. DE HAAN,*,†,‡ ASHLEY L. CORRIGAN,† MARGARET A. TOLBERT,‡ JOSE L. JIMENEZ,‡ STEPHANIE E. WOOD,†,‡ AND JACOB J. TURLEY†,‡

Department of Chemistry and Biochemistry, University of San Diego, and Cooperative Institute for Research in Environmental Sciences, and Department of Chemistry and Biochemistry, University of Colorado, Boulder

Received July 17, 2009. Revised manuscript received September 8, 2009. Accepted September 27, 2009.

Glyoxal and methylglyoxal are scavenged by clouds, where a fraction of these compounds are oxidized during the lifetime of the droplet. As a cloud droplet evaporates, the remaining glyoxal and methylglyoxal must either form low-volatility compounds such as oligomers and remain in the aerosol phase, or transfer back to the gas phase. A series of experiments on evaporating aqueous aerosol droplets indicates that over the atmospherically relevant concentration range for clouds and fog (4−1000 μM), 33 ± 11% of glyoxal and 19 ± 13% of methylglyoxal remains in the aerosol phase while the remainder evaporates. Measurements of aerosol density and time-dependent AMS signal changes are consistent with the formation of oligomers by each compound during the drying process. Unlike glyoxal, which forms acetal oligomers, exact mass AMS data indicates that the majority of methylglyoxal oligomers are formed by aldol condensation reactions, likely catalyzed by pyruvic acid, formed from methylglyoxal disproportionation. Our measurements of evaporation fractions can be used to estimate the global aerosol formation potential of glyoxal and methylglyoxal via self-reactions at 1 and 1.6 Tg C yr^{-1}, respectively. This is a factor of 4 less than the SOA formed by these compounds if their uptake is assumed to be irreversible. However, these estimates are likely lower limits for their total aerosol formation potential because oxidants and amines will also react with glyoxal and methylglyoxal to form additional low-volatility products.

Introduction

Tropospheric submicrometer aerosol particles usually contain significant organic material (*1, 2*), and this material impacts particle growth (*3*) and subsequent cloud condensation (*4*). Conversely, cloud processing (the passage of gases and aerosol through the aqueous phase in clouds) is now recognized as an important source of secondary organic aerosol (SOA) (*5*). In this process, water-soluble gases are scavenged by cloud droplets, where they may be converted to low-volatility compounds via oxidation (*6*) or by oligomerization reactions triggered by oxidation (*7*) or droplet evaporation (*8*).

Highly water-soluble α-dicarbonyl compounds are suspected of producing large amounts of SOA via aerosol uptake (*9*) and cloud processing (*10*). Assuming glyoxal and methylglyoxal are taken up irreversibly by clouds and aerosol with an uptake coefficient measured for glyoxal ($\alpha = 0.0029$ (*11*)), it has been estimated that 11 Tg C yr^{-1} SOA would form (*10*), an amount equal to about one-half of recent estimates of the total primary organic aerosol emissions from biomass burning (*12*). Almost 70% of this amount is due to cloud processing of methylglyoxal.

The value of the initial uptake coefficient of methylglyoxal is subject to considerable uncertainty (*13, 14*), and the assumption of irreversible uptake for either α-dicarbonyl compound is controversial (*11, 13, 15, 16*). Aqueous-phase oxidation of α-dicarbonyl compounds is the best-characterized pathway to SOA formation (and therefore irreversible uptake). Both glyoxal and methylglyoxal react with OH radical at similar rates ($k = 1.1 \times 10^9$ M^{-1} s^{-1} and E/R = 1516 and 1600 K, respectively) (*17, 18*), producing low-volatility reaction products including oligomers (*7, 19*). However, since the lifetime of a typical cloud droplet is 10 min, only ∼5% of the α-dicarbonyl compounds would be oxidized during this time if $[\bullet OH] = 1 \times 10^{-13}$ M (*20, 21*) and $T = 280$ K. Cloud droplet evaporation may then trigger further oligomerization reactions of the remaining α-dicarbonyl compounds. Drying droplets containing 1 M α-dicarbonyls have been shown to oligomerize fast enough that 100% of the glyoxal and 60% of the methylglyoxal is trapped in the condensed phase (*8*). In atmospheric cloud droplets, where concentrations of both compounds are in the μM range (*22*−*27*), the rates of self-reactions should decrease. However, other nucleophiles present in cloudwater, such as amines (*28*), will also react with glyoxal (*29, 30*) and likely with methylglyoxal. Reactions between glyoxal and amines, like glyoxal self-reactions, are greatly accelerated by droplet drying (*29*).

The goals of the current study are to quantify the aerosol-forming potential of methylglyoxal and glyoxal via self-reactions during simulated cloud processing, and experimentally verify the chemistry responsible for the observed behavior. We use vibrating orifice aerosol generation (VOAG)/scanning mobility particle sizing (SMPS) experiments to show that over the concentration range 4−1000 μM, nearly constant proportions of methylglyoxal (19 ± 13%) and glyoxal (33 ± 11%) remain behind in the residual aerosol particles produced when aqueous droplets evaporate. Oligomer formation triggered by droplet drying appears to be the dominant process responsible for this production of aerosol-phase material. We compare high-resolution time-of-flight aerosol mass spectrometry (HR-ToF-AMS) data with electrospray ionization (ESI) MS data from bulk solutions to show that methylglyoxal forms oligomers largely by aldol condensation, as predicted by theory (*31, 32*). Finally, the effective densities of glyoxal and methylglyoxal oligomers are determined using the AMS/SMPS method (*33*). For glyoxal, this density matches that of glyoxal trimer dihydrate (*16*), as expected.

Experimental Section

We generated 1.0 M stock solutions by overnight hydrolysis of solid glyoxal trimer dihydrate (Sigma-Aldrich) (*15*) and by dilution from 40% w/w methylglyoxal solution (MP Biomedicals). These were stored in the dark at 4 °C under

* Corresponding author e-mail: ddehaan@sandiego.edu.
† University of San Diego.
‡ University of Colorado.

10.1021/es902152t CCC: $40.75
Published on Web 10/07/2009

nitrogen to minimize oxidation reactions. Stock solutions were diluted in D_2O for analysis by NMR (Varian, 400 MHz), in 18-MΩ reagent-grade H_2O (NERL Diagnostics) for VOAG experiments, and in HPLC-grade H_2O (Honeywell) for other experiments. Solution pH was measured with a Corning 320 pH meter and Sensorex S200C sensor.

The fractions of glyoxal and methylglyoxal that evaporate from droplets were determined in VOAG/SMPS experiments (Supporting Information (SI) Scheme S01). Monodisperse 22-μm-diameter aqueous droplets were generated from glyoxal and methylglyoxal solutions (4−100 μM) in reagent-grade water by VOAG (TSI model 3450, 10 μm orifice, liquid flow rate $Q = 0.09$ mL/min, vibration frequency $f = 280$ kHz). All solution contact with glass was avoided in order to minimize leaching of nonvolatile impurities. Immediately after generation, droplets were dispersed at room temperature into a 10 L/min flow of dry, prepurified N_2 to minimize coagulation, achieving number concentrations below 2×10^3 cm^{-3}. Droplets passed through an in-line neutralizer (NRD model P2021−1000, Po-210), a series of 4 L gas dryers, and a diffusion dryer before SMPS analysis (TSI 3080/3081/3010, 0.071 cm impactor). Excess flow was vented through a HEPA filter. RH was monitored at the vent (Vaisala HMT337) and ranged from 18 to 30%. Drying times were varied from 0.5 to 3 min by changing the number of in-line gas dryers in the flow path. Low concentration runs preceded higher concentration runs each day to avoid contamination of low concentration runs by α-dicarbonyls from prior experiments desorbing from the walls (*13*). Higher concentration (100 μM) runs could produce gas-phase dicarbonyl concentrations as high as 14 ppb.

Typical measured aerosol size distributions exhibited a distinct peak with geometric standard deviations of ∼1.1. Geometric means of these peaks were compared with those generated from water, which was run before every α-dicarbonyl solution, to determine the increase in residual particle size and volume due to the organic solute, $\Delta V_{meas} = V_{org} - V_{H_2O}$. These volume increases were divided by the calculated residual volume of the organic solute present in the original wet droplet, V_{calc} (eq 1) to find the aerosol-phase recovery, $R_{aerosol}$.

$$V_{calc} = \frac{V_{wet} C_{org} MW_{monomer}}{\rho_{eff}} \quad (1)$$

where V_{wet} is the wet drop volume generated by VOAG, C_{org} is the organic concentration in the droplet-generating solution (moles cm^{-3}), $MW_{monomer}$ is the average monomer mass in the residual particle (g mole^{-1}), and ρ_{eff} is the effective density of the resulting aerosol particles (g cm^{-3}). The VOAG wet drop size was verified with SMPS measurements of 37 μM NaCl solutions, resulting in NaCl aerosol recoveries of 100% within experimental error ($R_{aerosol} = 106 \pm 8\%$ if spherical and $91 \pm 7\%$ using $\rho_{eff,\,NaCl} = 1.85$ to correct for nonspherical particle shapes (*34*)). Since glyoxal oligomerizes into a trimer dihydrate with a mass of 210 amu, $MW_{glyoxal\ monomer} = 210/3 = 70$ amu. In this work, we find that methylglyoxal oligomers have $MW_{MeGly\ monomer} = (65 \pm 3)$ amu. Effective density measurements are described below which suggest minimal aerosol water content. The measured nonvolatile fraction of impurities in solvent water varied between 0.1 and 0.5 ppm and was the major source of uncertainty in quantifying the amount of glyoxal or methylglyoxal recovered in residual aerosol.

In order to link VOAG/SMPS data with previous quantitative evaporation experiments performed at 1.0 M (*8*), analogous SMPS evaporation experiments were also performed at intermediate (mM) concentrations with polydisperse aerosol held for 5−20 min in the chamber at >55% RH (SI Scheme S02). In some experiments dry air was added to reduce RH to 25−40%, but this addition had no apparent effect on size distributions. Aerosol particles were generated using ultrasonic or pneumatic nebulization and solute concentrations in the range 1−20 mM, and SMPS size distributions of the residual organic aerosol were recorded. Aerosol coagulation rates were minimized by keeping number concentrations at 2×10^5 cm^{-3} or less. Wet drop size distributions were back-calculated from residual NaCl aerosol size distributions accounting for nonsphericity (*34*), and were assumed to be invariant for a given aerosol generation technique. V_{calc} was determined using eq 1, this time integrating across the size distribution. In the mM concentration range, volume contributions from nonvolatile solvent impurities are negligible and $\Delta V_{meas} \cong V_{org}$. Total number density for organic aerosol were normalized to NaCl number density to correct for atomizer variability.

To determine effective particle densities of residual glyoxal and methylglyoxal aerosol, SMPS and quadrupole (Q)-AMS, Aerodyne (*35*)) size distributions were measured simultaneously after both instruments were size calibrated using polystyrene latex spheres with nominal diameters between 100 and 700 nm (Nanosphere size standards, Thermo Scientific). Droplets were generated by pneumatic nebulization of ∼15 mM solutions. Effective density is equal to the actual density of aerosol particles if they are spherical (*33*). Glycine (Sigma-Aldrich) aerosol density was also measured to test the method (SI Scheme S02).

Atomic force microscopy (AFM) was used to verify that dried glyoxal aerosol particles were spherical. Monodisperse aerosol particles were produced by VOAG from a 50 μM glyoxal solution (SI Scheme S01). The aerosol particles were dried for 1 min in a flowing system at ∼25% RH and collected on an impactor, where further drying under ambient conditions occurred for an hour. AFM SiO_x/Si(100) substrates that were cleaned using sequential sonication in toluene, acetone, and methanol were used as impaction plates. AFM images were obtained in tapping mode using a Veeco Dimension 3100 AFM with a Nanoscope IVa controller. Silicon tips (Nanosensors PPP-FMR) with a spring constant of 2.5−4 N m^{-1} were used.

A combination of AMS and electrospray ionization (ESI)-MS were used to study methylglyoxal oligomerization. In AMS experiments, stock solution were diluted and nebulized pneumatically (TSI model 9300) or ultrasonically (*29*) into a dilute aqueous aerosol. This aerosol was dried either quickly by passing through a diffusion dryer (SI Scheme S03), or slowly in a collapsible 300 L Teflon chamber held between 60 and 95% relative humidity (RH) (SI Scheme S02). The latter conditions are meant to simulate atmospheric conditions just outside a cloud. The resulting residual or cloud-processed aerosol particles were analyzed by a combination of Q-AMS, high-resolution time-of-flight (HR-ToF)-AMS (Aerodyne (*36*)), and SMPS over the size range 10−1000 nm. Heavy fragmentation of analyte molecules is observed in both AMS instruments. In ESI-MS experiments (a soft ionization method causing little fragmentation), 150 μL aliquots of 50 mM methylglyoxal solutions were dried under ambient conditions, redissolved in 18 MΩ water to reach 1 mg/mL, and analyzed without any chromatographic preseparation (SI Scheme S04, Thermo-Finnigan LCQ Advantage, syringe pump at 2.5 μL/min with ESI nozzle voltage = +4.3 kV, medical N_2 sheath gas flow = 25, capillary temp = 250 °C). Q-AMS and ESI-MS were operated slightly above unit mass resolution, whereas HR-ToF-AMS allowed chemical formulas to be determined by exact mass.

Results and Discussion

VOAG experiments were used to determine the amount of drying time necessary for 22 μm diameter monodisperse

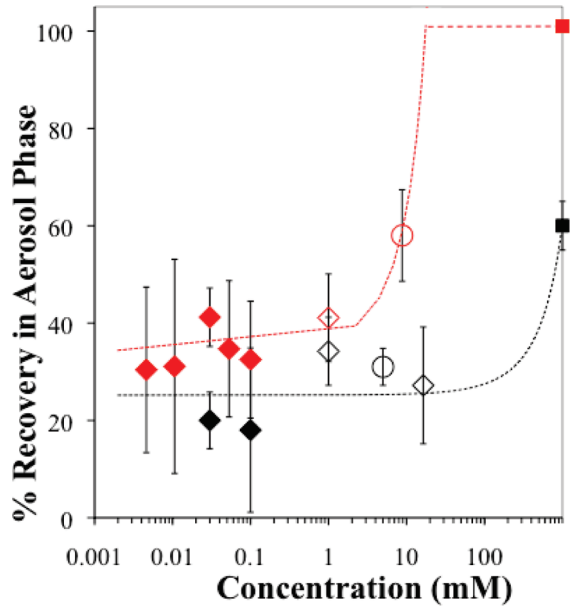

FIGURE 1. Percent methylglyoxal (black) and glyoxal (red) recovered in the condensed phase as a function of carbonyl concentration in original wet droplets. Filled diamonds: averages of VOAG experiments where droplets were dried by decreasing RH from 50 to 25% over 2 min before SMPS measurements. Open symbols: polydisperse aerosol experiments where aerosol generated by ultrasonic nebulization (circles) or pneumatic nebulization (diamonds) was dried at RH > 70% for 10 min or more before SMPS measurements. Filled squares: bulk 1 μL droplets, RH > 95%, ref (*8*). Exponential fits are shown. Glyoxal experiment at 1 M is not included in fit.

droplets initially containing 30 μM glyoxal or methylglyoxal to achieve stable residual particle sizes (SI Figure S01). For both α-dicarbonyls, differences in residual particle sizes were statistically insignificant as drying times increased beyond 2 min at 18−30% RH. All VOAG evaporation experiments were therefore conducted with drying times of 2 min or more.

Results from VOAG and chamber evaporation experiments on aqueous droplets initially containing 0.004−20 mM concentrations of one α-dicarbonyl compound are summarized in Figure 1, shown with our published high-RH, high-concentration data. Residual SMPS size distribution data has been converted to percentages of α-dicarbonyl recovered in the aerosol phase, plotted as a function of initial solute concentrations. Loeffler et al. (2006) (*8*) showed that at 1 M methylglyoxal concentrations, recovery in the aerosol phase actually goes up as RH drops. Thus, it is highly unlikely that the differences in RH among the measurements could cause the observed trend, which is in the opposite direction. We also note that different atomization techniques produce wet droplets with different size ranges (Bulk droplets (*8*) ≫ VOAG > ultrasonic nebulization > pneumatic nebulization). However, the data does not follow this trend. Thus it is both more plausible and expected that aerosol-phase recoveries depend on concentration.

Aerosol-phase recoveries appear to be nearly constant for each compound for initial aqueous concentrations ≤1 mM, with 33 ± 11% of glyoxal and 19 ± 13% of methylglyoxal recovered in the aerosol phase. This aerosol production must be due to either pre-existing, nonvolatile impurities in the glyoxal and methylglyoxal solutions or to the formation of nonvolatile products in reactions that occur as water evaporates from the droplets. These possibilities are explored in the experiments described below.

Products such as oxalic and pyruvic acids form when glyoxal and methylglyoxal are oxidized by hydroxyl radicals in aqueous solution (*19, 20*). Stock solutions of methylglyoxal (0.5 M) and glyoxal in D_2O were analyzed in ^{1}H-, ^{13}C-, and heteronuclear multiple quantum coherence (HMQC)-NMR experiments in order to identify and quantify such impurities. No oxalic acid was observed by ^{13}C NMR in either solution. (It is not observable by the other two techniques.) For methylglyoxal, peak assignments are listed in SI Table S01. Monohydrate and dihydrate methylglyoxal monomers were present at a 55:45 ratio, while unhydrated methylglyoxal was not detected, consistent with previous work (*37*) and with computations (*32*). Peaks assigned to specific acetal oligomers (*37*) were not observed in D_2O solutions, consistent with previous studies. Several new peaks were observed (SI Figure S02 and Table S01), along with hydroxyacetone and pyruvic acid hydrate, the twin products of methylglyoxal disproportionation (SI Scheme S05) occurring either by electrocyclic ring-opening (*38*) of an acetal dimer with a dioxolane ring structure, or by Cannizzaro reaction (*39*). ^{1}H NMR peak integrations in the methyl group region (1.0−2.3 ppm) indicate that the solution contained 53% monomers, 37% dimers and oligomers, and equimolar amounts (≤5%) of hydroxyacetone and pyruvic acid hydrate. The measured pH of a 10 mM methylglyoxal solution was 3.7, consistent with a 2% pyruvic acid impurity. Pyruvic acid at these concentrations is itself responsible for no more than 3% of the aerosol formation observed for methylglyoxal solutions, but it likely serves as an acid catalyst for aldol condensation reactions in our experiments. Hydroxyacetone is volatile and will not contribute to the observed aerosol yield unless it participates in oligomerization reactions.

Effective particle densities were extracted from SMPS and Q-AMS size distributions measured for glycine, glyoxal, and methylglyoxal aerosol dried in the chamber. The measured effective density of solid glycine aerosol generated from 4 mM solution was 1.18 ± 0.06 g cm^{-3} (SI Figure S03), consistent with the known density of solid glycine (1.16 g cm^{-3}), indicating that particles were spherical. SI Figure S04 shows that residual glyoxal aerosol generated from 18 mM solution has an effective density of 1.71 ± 0.02 g cm^{-3}. This overlaps the recently measured density range of solid glyoxal trimer dihydrate pellets (1.67 to 1.70 g cm^{-3}) (*16*), consistent with dry, spherical aerosol made of this substance or of other oligomers with the same density. SI Figure S05 shows an AFM image of dried, spherical glyoxal aerosol particles generated by VOAG. An 18 mM glyoxal solution at equilibrium should contain 99.5% monomers, given a dimerization constant $K_{dimer} = 0.56$ (*40, 41*). This corresponds to a negligible aerosol yield of 0.5% due to pre-existing oligomers in the starting solution. The observed 33 ± 11% yield starting from lower initial concentrations can therefore be consistently attributed only to glyoxal oligomer formation during droplet drying. Previous work has shown that glyoxal acetal oligomers can form within minutes in drying 1 μL droplets (*8*) and aerosol particles (*11*). While our measured aerosol yields are significantly less than those observed for 1 M solutions (*8*), we note that some concentration dependence is expected for oligomer formation.

As shown in SI Figure S06, the effective density of residual methylglyoxal aerosol generated from 16 mM solution is 1.9 ± 0.1 g cm^{-3}. This effective density is comparable to glyoxal oligomers, and is incompatible with spherical or nonspherical particles composed mainly of the methylglyoxal oxidation product pyruvic acid ($\rho = 1.26$) or of water. Furthermore, as will be shown below, Q-AMS signals assigned to oligomer species increased during droplet drying even as all other signals declined due to wall losses. Thus, we conclude that the measured density, and by extension the 19 ± 13% aerosol yield, is due to oligomers formed during the droplet drying process.

The oligomers formed in drying methylglyoxal droplets and bulk solutions were chemically characterized using mass

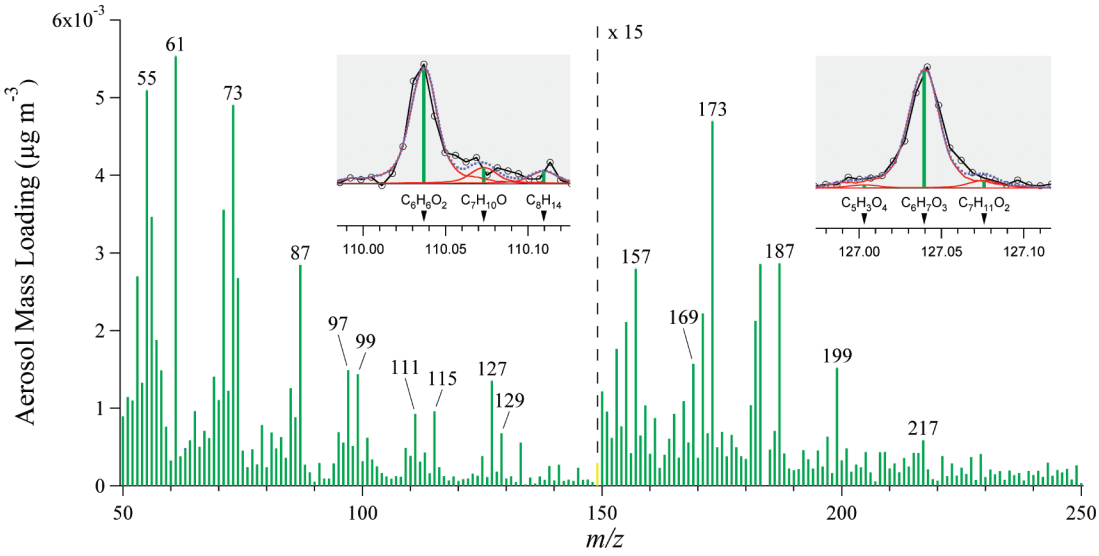

FIGURE 2. HR-ToF-AMS stick spectrum of methylglyoxal aerosol generated from 4 mM solution by pneumatic nebulization at 15 psi. Aerosol passed through diffusion dryer en route to AMS. The *y*-axis of the data on the right has been expanded by a factor of 15. Green: organic compounds. Red: sulfate. Yellow: instrument background signals. Insets: high-resolution fits at *m/z* 110 and 127, with data in purple, individual ion peak fits in red and the sum of fitted ions in dotted blue.

spectrometry data. When methylglyoxal solutions are pneumatically nebulized through a diffusion dryer, or ultrasonically nebulized and dried in a chamber at 60% RH for ~20 min, HR-ToF-AMS analysis detects many peaks at m/z ratios higher than the molecular mass of the reactant (Figure 2). Signal strengths allow the accurate assignment of high-resolution peaks below m/z 200 to unique molecular formulas. Prominent peaks appear at m/z 87 ($C_4H_7O_2^+$), 97 and 99 ($C_5H_xO_2^+$), 111 ($C_6H_7O_2^+$), 115 ($C_5H_7O_3^+$), 125 ($C_7H_9O_2^+$ and $C_6H_5O_3^+$), 127 and 129 ($C_6H_xO_3^+$). These fragment species can be attributed to oligomers formed from methylglyoxal and, in some cases, methylglyoxal and hydroxyacetone.

The O/C ratios of C_4-C_6 fragments measured by HR-ToF-AMS (SI Table S02) were used to distinguish between different classes of oligomers. Potential acetal methylglyoxal dimers analogous to glyoxal dimers have O/C ratios of 0.83 or more, but could decline to 0.67 after water loss by EI fragmentation. Less than 3% of the total C_4-C_6 fragment signals have O/C ratios ≥0.67. Acetal dimers formed from methylglyoxal and hydroxyacetone could, after water loss, have O/C ratios as low as 0.5 (SI Scheme S06), consistent with 60% of the total C_4-C_6 fragment signal. On the other hand, possible dimers formed by aldol condensation (Scheme 1) have the lowest O/C ratios and are consistent with over 99% of the total C_4-C_6 fragment signal. Thus, aldol condensation products could be responsible for 40−99.7% of the observed signal in methylglyoxal samples.

Because of heavy analyte fragmentation in the AMS, a bulk methylglyoxal solution that was dried and redissolved in water was analyzed by ESI-MS in order to determine the extent of oligomer formation. Figure 3 shows multiple ESI-MS peaks separated by $\Delta m/z$ 18, 56, 72, and 128 out to at least m/z 585. Oligomers seen by both AMS $(M-1)^+$ and ESI-MS $(M+1)^+$ are m/z 110 ($C_6H_6O_2^+$), 128 ($C_6H_8O_3^+$), and 168 ($C_8H_8O_4^+$), which are consistent with aldol condensation or acetal products of methylglyoxal and hydroxyacetone reactions. Given the repeating pattern of peaks that differ by m/z 56, 72, and 128, and our ability to accurately assign these fragments using HR-ToF-AMS to C_3H_4O, $C_3H_4O_2$, and $C_6H_8O_3$, respectively, we can assign molecular formulas to larger peaks made from these building blocks with a high degree of confidence (*30*). These include most of the labeled peaks in Figure 3, including m/z 201, 257, 273, 313, 369, 385, 441, 457, 513, and 585. Several other prominent peaks are reached by

SCHEME 1. Methylglyoxal Oligomerization Reaction Products Consistent with MS Data (Hydration of Carbonyl Functional Groups Not Shown)

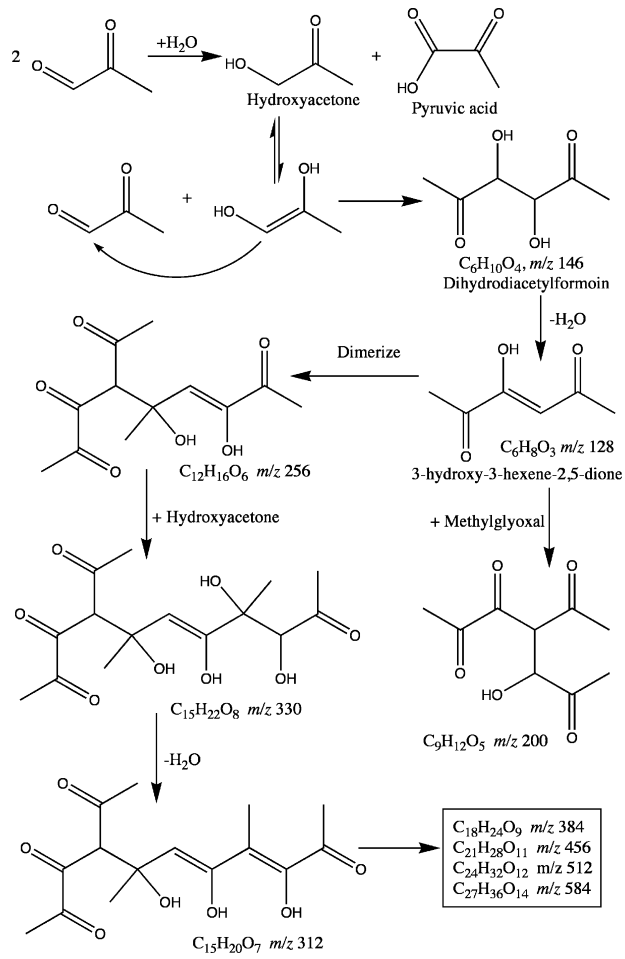

the addition of single water molecules to peaks listed above: m/z 147, 331, 403, and 531.

These repeating series of MS peaks are consistent with aldol condensation products of $C_6H_8O_3$ (m/z 128), meth-

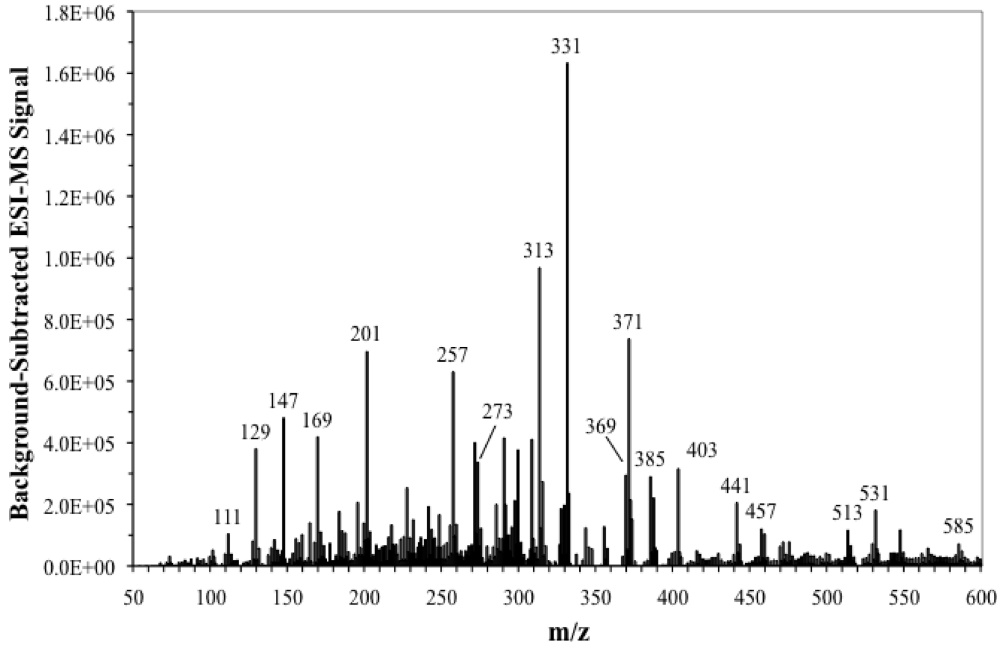

FIGURE 3. Positive-mode ESI-MS spectrum of bulk 50 mM methylglyoxal solution after drying/redissolving cycle. Background spectrum of water has been subtracted using linearly varying scaling to minimize instrument background peaks at *m/z* 304, 371, and 445.

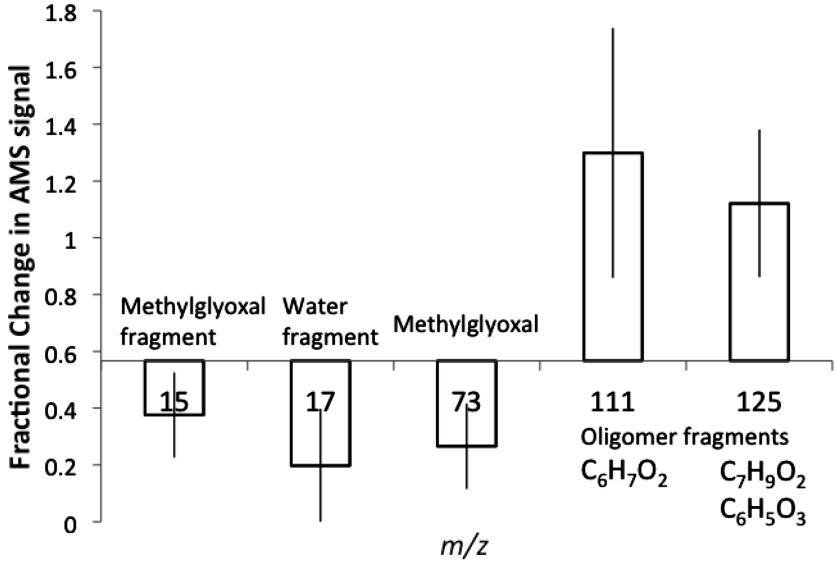

FIGURE 4. Changes in AMS signals observed during the drying of aerosol droplets formed by pneumatic nebulization of 16 mM methylglyoxal solution at 60% RH. Peak identifications were confirmed by HR-ToF-AMS; the peak at *m/z* 125 had a contribution from two different formulas. Average loss in AMS signal due to chamber wall losses was 42%, which is used as the *x*-axis. Bars pointing downward represent AMS signal masses that declined faster than this. Peaks that changed by the greatest percentages relative to the average are shown here.

ylglyoxal and hydroxyacetone units (Scheme 1). Hydroxyacetone can react with methylglyoxal in an (pyruvic) acid-catalyzed aldol condensation reaction to form dihydrodiacetylformoin ($C_6H_{10}O_4$, m/z 146). This product has been previously identified in methylglyoxal solutions treated with zinc and acid (*42*). In acid, 3-hydroxy-3-hexene-2,5-dione ($C_6H_8O_3$, m/z 128) is the major product of the subsequent reaction (*42*). After this, continued aldol additions of methylglyoxal and hydroxyacetone can form multiple structures with the correct chemical formulas, examples of which are shown in Scheme 1. An oligomer formed from five methylglyoxal monomers and four hydroxyacetone monomers matches the chemical formula of the largest peak in the series at m/z 584 ($C_{27}H_{36}O_{14}$).

Since NMR measurements indicated that methylglyoxal stock solutions contained ~37% oligomers, but dilute solutions produced only a 19 ± 13% aerosol yield, it is clear that at least some of the oligomers observed in stock solutions are in equilibrium with methylglyoxal monomer and revert to the monomer upon dilution. However, because pre-existing oligomers would not be present in cloudwater it was necessary to determine whether the methylglyoxal oligomers observed by AMS and ESI-MS (and likely responsible for the observed 19 ± 13% aerosol yields) were pre-existing or were formed during the aerosol drying process. To this end, changes in AMS signals during the density experiment described above were analyzed. Figure 4 shows [final signal]/[initial signal] ratios for five masses that showed the greatest

changes relative to the average signal decline observed due to aerosol wall losses. Large decreases in m/z 15, 17, and 73 were observed, consistent with the loss of methylglyoxal (m/z 15, 73) and water (fragment m/z 17) due to either reaction or evaporation. Significant increases were observed at m/z 111 and 125, which we have identified as $C_6H_7O_2^+$ and $[C_7H_9O_2^+ + C_6H_5O_3^+]$ oligomers and fragments using HR-ToF-AMS. These observations are consistent with significant oligomer formation during the 45 min time scale of this aerosol evaporation experiment.

Past work has shown that glyoxal can be trapped in the aerosol phase during droplet drying due to acetal oligomer formation (*8*). At atmospherically relevant concentrations, we find that this process traps 33 ± 11% of the glyoxal in the aerosol phase. Methylglyoxal, with a Henry's law constant 11 times smaller than glyoxal (3.2×10^4 vs 3.6×10^5, respectively, in seawater at 25 °C (*43*)), evaporates more readily, consistent with the lower 19 ± 13% aerosol yield measured here. These numbers are near the average gas/particle partitioning ratios measured in a remote forest for these compounds: 46% for glyoxal and 36% for methylglyoxal (*44*). While we cannot rule out a contribution to our measured aerosol yields from pre-existing oligomers in the methylglyoxal stock solution, AMS observations indicate significant oligomer formation during droplet drying. Although it appears that aldol condensations occur only in methylglyoxal solutions (perhaps due to the presence of hydroxyacetone), both glyoxal and methylglyoxal can be expected to form aerosol via oligomer formation in evaporating cloud droplets. Under tropospheric conditions, aldol condensation reactions are likely to be catalyzed by ammonium ions (*45*), which could increase the rate of formation of methylglyoxal oligomers relative to dehydration and evaporation processes. This could potentially increase the fraction that forms aerosol during cloud processing relative to our measurements conducted in the absence of ammonium salts.

As a first approximation, our measurements of concentration-independent aerosol recoveries across most of the concentration range of glyoxal and methylglyoxal in atmospheric cloudwater can be used to provide better estimates of SOA formation by these compounds. The uptake of glyoxal and methylglyoxal into clouds and fog can lead to, first, aqueous-phase oxidation, whose rates depend on highly variable hydroxyl radical concentrations. Subsequently, as cloud droplets evaporate, 33 ± 11% and 19 ± 13% of the remaining glyoxal and methylglyoxal, respectively, will form oligomers, and therefore SOA, due to self-reactions. These percentages can be multiplied by the estimates of Fu et al. (*10*) to show that, ignoring oxidation and reactions with other nucleophiles, glyoxal and methylglyoxal can produce 1 and 1.6 Tg C/yr SOA, respectively, via self-reaction to form oligomers. This is a factor of 4 lower than the estimated SOA production from glyoxal and methylglyoxal when evaporation from cloud droplets was neglected (*10*). However, these estimates are likely lower limits because oxidation, which takes place prior to oligomer formation, will form additional low-volatility products during each cloud cycle (*46*). In addition, the presence of amino compounds (*28*) and hydroxyacetone (*27*) in clouds may increase the amount of SOA formed.

Acknowledgments

We thank Miriam A. Freedman for assistance with AFM analysis, which was performed at the University of Colorado's Nanomaterials Characterization Facility. This work was supported by NSF grant ATM-0749145. D.D.H. was supported by a CIRES Fellowship.

Supporting Information Available

Graphs of particle size vs drying time, ^{1}H NMR methylglyoxal spectrum and peak assignments, HR-ToF-AMS C_4-C_6 methylglyoxal oligomer fragments detected, an AFM image of glyoxal aerosol, and aerosol density fits. This material is available free of charge via the Internet at http://pubs.acs.org.

Literature Cited

(1) Murphy, D. M. Single-particle mass spectrometry of tropospheric aerosol particles. *J. Geophys. Res.* **2006**, *111*, D23S32, DOI: 10.1029/2006JD007340.

(2) Zhang, Q.; et al. Ubiquity and dominance of oxygenated species in organic aerosols in anthropogenically-influenced Northern Hemisphere midlatitudes. *Geophys. Res. Lett.* **2007**, *34*, L13801, DOI: 10.1029/2007GL029979.

(3) Wehner, B.; et al. The contribution of sulfuric acid and non-volatile compounds on the growth of freshly formed atmospheric aerosols. *Geophys. Res. Lett.* **2005**, *32*, L17810.

(4) Charlson, R. J.; et al. Reshaping the theory of cloud formation. *Science* **2001**, *292*, 2025–2026.

(5) Carlton, A. G.; et al. CMAQ model performance enhanced when in-cloud secondary organic aerosol is included: comparisons of organic carbon predictions with measurements. *Environ. Sci. Technol.* **2008**, *42*, 8798–8802.

(6) Blando, J. D.; Turpin, B. J. Secondary organic aerosol formation in cloud and fog droplets: A literature evaluation of plausibility. *Atmos. Environ.* **2000**, *34*, 1623–1632.

(7) Altieri, K. E.; et al. Oligomers formed through in-cloud methylglyoxal reactions: chemical composition, properties, and mechanisms investigated by ultra-high resolution FT-ICR mass spectrometry. *Atmos. Environ.* **2008**, *42*, 1476–1490.

(8) Loeffler, K. W.; et al. Oligomer formation in evaporating aqueous glyoxal and methyl glyoxal solutions. *Environ. Sci. Technol.* **2006**, *40*, 6318–6323.

(9) Volkamer, R.; et al. A missing sink for gas-phase glyoxal in Mexico City: formation of secondary organic aerosol. *Geophys. Res. Lett.* **2007**, *34*, L19807.

(10) Fu, T.-M.; et al. Global budgets of atmospheric glyoxal and methylglyoxal, and implications for formation of secondary organic aerosols. *J. Geophys. Res.* **2008**, *113*, D15303.

(11) Liggio, J.; Li, S.-M.; McLaren, R. Reactive uptake of glyoxal by particulate matter. *J. Geophys. Res.* **2005**, *110*, D10304.

(12) Hallquist, M.; et al. The formation, properties and impact of secondary organic aerosol: current and emerging issues. *Atmos. Chem. Phys.* **2009**, *9*, 5155–5235.

(13) Kroll, J. H.; et al. Chamber studies of secondary organic aerosol growth by reactive uptake of simple carbonyl compounds. *J. Geophys. Res.* **2005**, *110*, D23207.

(14) Zhao, J.; et al. Heterogeneous reactions of methylglyoxal in acidic media: implications for secondary organic aerosol formation. *Environ. Sci. Technol.* **2006**, *40*, 7682–7687.

(15) Hastings, W. P.; et al. Secondary organic aerosol formation by glyoxal hydration and oligomer formation: humidity effects and equilibrium shifts during analysis. *Environ. Sci. Technol.* **2005**, *39*, 8728–8735.

(16) Galloway, M. M.; et al. Glyoxal uptake on ammonium sulphate seed aerosol: reaction products and reversibility of uptake under dark and irradiated conditions. *Atmos. Chem. Phys.* **2009**, *9*, 3331–3345.

(17) Buxton, G. V.; Malone, T. N.; Salmon, G. A. Oxidation of glyoxal initiated by OH in oxygenated aqueous solution. *J. Chem. Soc., Faraday Trans.* **1997**, *93*, 2889–2891.

(18) Ervens, B.; Gligorovski, S.; Herrmann, H. Temperature-dependent rate constants for hydroxyl radical reactions with organic compounds in aqueous solutions. *Phys. Chem. Chem. Phys.* **2003**, *5*, 1811–1824.

(19) Carlton, A. G.; et al. Atmospheric oxalic acid and SOA production from glyoxal: results of aqueous photooxidation experiments. *Atmos. Environ.* **2007**, *41*, 7588–7602.

(20) Ervens, B.; et al. A modeling study of aqueous production of dicarboxylic acids: 1. Chemical pathways and speciated organic mass production. *J. Geophys. Res.* **2004**, *109*, D15205.

(21) Deguillaume, L.; Leriche, M.; Chaumerliac, N. Impact of radical versus non-radical pathway in the Fenton chemistry on the redox cycle in clouds. *Chemosphere* **2005**, *60*, 718–724.

(22) Steinberg, S.; Kaplan, I. R. The determination of low molecular weight aldehydes in rain, fog and mist by reversed phase liquid chromatography of the 2,4-dinitrophenylhydrazone derivatives. *Int. J. Environ. Anal. Chem.* **1984**, *18*, 253–266.

(23) Igawa, M.; Munger, J. W.; Hoffmann, M. R. Analysis of aldehydes in cloud- and fogwater samples by HPLC with a postcolumn reaction detector. *Environ. Sci. Technol.* **1989**, *23*, 556–561.

(24) Collett, J. L. J.; et al. Intensive studies of Sierra Nevada cloud water chemistry and its relationship to precursor aerosol and gas concentrations. *Atmos. Environ. A* **1990**, *24*, 1741–1757.
(25) Munger, J. W.; et al. Formaldehyde, glyoxal, and methylglyoxal in air and cloudwater at a rural mountain site in central Virginia. *J. Geophys. Res.* **1995**, *100*, 9325–9333.
(26) Matsumoto, K.; Kawai, S.; Igawa, M. Dominant factors controlling concentrations of aldehydes in rain, fog, dew water, and in the gas phase. *Atmos. Environ.* **2005**, *39*, 7321–7329.
(27) van Pinxteren, D.; et al. Schmucke hill cap cloud and valley stations aerosol characterisation during FEBUKO (II): organic compounds. *Atmos. Environ.* **2005**, *39*, 4305–4320.
(28) Zhang, Q.; Anastasio, C. Free and combined amino compounds in atmospheric fine particles ($PM_{2.5}$) and fog waters from Northern California. *Atmos. Environ.* **2003**, *37*, 2247–2258.
(29) De Haan, D. O.; et al. Atmospheric condensed-phase reactions of glyoxal with amino acids. *Environ. Sci. Technol.* **2009**, *43*, 2818–2824.
(30) De Haan, D. O.; Tolbert, M. A.; Jimenez, J. L. Atmospheric condensed-phase reactions of glyoxal with methylamine. *Geophys. Res. Lett.* **2009**, *36*, L11819.
(31) Barsanti, K. C.; Pankow, J. F. Thermodynamics of the formation of atmospheric organic particulate matter by accretion reactions—2. Dialdehydes, methylglyoxal, and diketones. *Atmos. Environ.* **2005**, *39*, 6597–6607.
(32) Krizner, H. E.; De Haan, D. O.; Kua, J. Thermodynamics and kinetics of methylglyoxal dimer formation: A computational study. *J. Phys. Chem. A* **2009**, *113*, 6994–7001.
(33) Jimenez, J. L.; et al. New particle formation from photooxidation of diiodomethane (CH_2I_2). *J. Geophys. Res.* **2003**, *108*, 4318.
(34) Zelenyuk, A.; et al. A new real-time method for determining particles' sphericity and density: application to secondary organic aerosol formed by ozonolysis of α-pinene. *Environ. Sci. Technol.* **2008**, *42*, 8033–8038.
(35) Canagaratna, M. R.; et al. Chemical and microphysical characterization of ambient aerosols with the Aerodyne aerosol mass spectrometer. *Mass Spectrom. Rev.* **2007**, *26*, 185–222.
(36) DeCarlo, P. F.; et al. Field-deployable, high-resolution, time-of-flight aerosol mass spectrometer. *Anal. Chem.* **2006**, *78*, 8281–8289.
(37) Nemet, I.; Vikic-Topic, D.; Varga-Defterdarovic, L. Spectroscopic studies of methylglyoxal in water and dimethylsulfoxide. *Bioorg. Chem.* **2004**, *32*, 560–570.
(38) Huyghues-Despointes, A.; Yaylayan, V. A. Retro-aldol and redox reactions of Amadori compounds: mechanistic studies with variously labeled D-[^{13}C]glucose. *J. Agric. Food Chem.* **1996**, *44*, 672–681.
(39) Wang, Y.; Ho, C.-T. Formation of 2,5-dimethyl-4-hydroxy-3(^{2}H)-furanone through methylglyoxal: a Maillard reaction intermediate. *J. Agric. Food Chem.* **2008**, *56*, 7405–7409.
(40) Chastrette, F.; et al. Study of aqueous glyoxal solutions by carbon-13 NMR. *Bull. Soc. Chim. Fr.* **1983**, 1−2 Pt. 2, 33−40.
(41) Fratzke, A. R.; Reilly, P. J. Thermodynamic and kinetic analysis of the dimerization of aqueous glyoxal. *Int. J. Chem. Kinet.* **1986**, *18*, 775–789.
(42) Buchi, G.; Demole, E.; Thomas, A. F. Synthesis of 2,5-dimethyl-4-hydroxy-2,3-dihydrofuran-3-one (furaneol), a flavor principle of pineapple and strawberry. *J. Org. Chem.* **1973**, *38*, 123–125.
(43) Zhou, X.; Mopper, K. Apparent partition coefficients of 15 carbonyl compounds between air and seawater and between air and freshwater; implications for air-sea exchange. *Environ. Sci. Technol.* **1990**, *24*, 1864–1869.
(44) Matsunaga, S.; Mochida, M.; Kawamura, K. Variation on the atmospheric concentrations of biogenic carbonyl compounds and their removal processes in the northern forest at Moshiri, Hokkaido Island in Japan. *J. Geophys. Res.* **2004**, *109*, D04302.
(45) Noziere, B.; Dziedzic, P.; Cordova, A. Products and kinetics of the liquid-phase reaction of glyoxal catalyzed by ammonium ions (NH_4^+). *J. Phys. Chem. A* **2009**, *113*, 231–237.
(46) Perri, M. J.; Seitzinger, S.; Turpin, B. J. Secondary organic aerosol production from aqueous photooxidation of glycolaldehyde: Laboratory experiments. *Atmos. Environ.* **2009**, *43*, 1487–1497.

ES902152T